Int J Thermophys (2009) 30:105–123
DOI 10.1007/s10765-008-0530-x

Characterizing the NRC Blackbody Sources for Radiation Thermometry from 150 °C to 962 °C

K. D. Hill · D. J. Woods

Published online: 18 November 2008

Abstract Validation of the various NRC blackbody sources below 962 °C has been hampered by the lack of a radiation thermometer with sufficient sensitivity and adequately small target size. Recently, progress was made in this area by having access to a NIST RT1550, a radiation thermometer operating at 1.55 μm with a thermoelectrically cooled InGaAs detector, a 3 mm nominal target size, a measuring range of 150 °C to 1064 °C, and a noise-equivalent temperature of 0.5 mK at 420 °C. Having the RT1550 for several months allowed sufficient time to intercompare our various blackbodies, both fixed-point and variable-temperature. It is these intralaboratory comparison results that are reported here.

Keywords Blackbody · Comparison · Emissivity

1 Introduction

In an earlier publication [1], we described our initial efforts to establish a blackbody-based calibration facility for radiation thermometers for the temperature range from −50 °C to 2500 °C. Validation of the performance of our various blackbody sources below 962 °C has been hampered by the lack of a radiation thermometer with sufficient sensitivity and adequately small target size (above 962 °C, our KE LP3 Linearpyrometer is well suited to the task). Our earlier publication illustrated the limitations of the Minolta/Land 300AF radiation thermometer for such work as a result of its rather large spot size (as revealed by size-of-source measurements), limited resolution, and noise at the level of a few tenths of a degree Celsius.

K. D. Hill (✉) · D. J. Woods
Institute for National Measurement Standards, National Research Council of Canada,
1200 Montreal Road, Bldg. M-36, Ottawa, ON, Canada K1A 0R6
e-mail: ken.hill@nrc-cnrc.gc.ca

Recently, we were fortunate in having in our laboratory for several months a newly developed NIST RT1550, a radiation thermometer operating at 1.55 µm with a thermoelectrically cooled InGaAs detector, a 3-mm nominal target size, a measuring range of 150 °C to 1064 °C, and a noise-equivalent temperature of 0.5 mK at 420 °C [2]. Access to the instrument for a sufficient period of time allowed us the opportunity to intercompare our various blackbodies, both fixed-point and variable-temperature, operating within the temperature range of the instrument. It is these intralaboratory comparison results at 1.55 µm that we are reporting.

To determine the radiance temperature of our blackbody sources, a "reference temperature" is first associated with the blackbody. In the case of our fixed-point blackbodies, the reference temperature is the temperature assigned to the phase transition of the filling material. For the variable-temperature blackbodies, the reference temperature is the temperature determined with a contact thermometer. The radiance temperature of a blackbody depends not only on this "reference temperature" but also on the effective emissivity of the blackbody, which is a function of the cavity geometry, the intrinsic emissivity of the material forming the walls of the cavity, and the temperature distribution along the cavity walls. In the sections to follow, we describe the geometry of our sources, present reflectance data (for opaque materials, emittance (ε) = 1 – reflectance (ρ)) for samples of material representative of the walls of the cavities, and show our measurements of wall temperature. These geometric and measured parameters are the input data for the STEEP3 Monte Carlo emissivity modeling software that we use to calculate the effective emissivity of the blackbody. The monochromatic radiance temperature, T_{Rad}, is given by

$$L(\lambda, T_{\mathrm{Rad}}) = \varepsilon(\lambda, T)\, L(\lambda, T) \tag{1}$$

where T is the "reference" or "true" temperature, λ is the wavelength of interest, and the ideal blackbody radiance, L, is given by

$$L(\lambda, T) = \frac{c_1}{\lambda^5 \left(\exp\left(\frac{c_2}{\lambda T}\right) - 1\right)} \tag{2}$$

The problem reduces to solving the following equality for T_{Rad},

$$\left(\frac{\exp\left(\frac{c_2}{\lambda T}\right) - 1}{\exp\left(\frac{c_2}{\lambda T_{\mathrm{Rad}}}\right) - 1}\right) = \varepsilon \tag{3}$$

For the values of λ, T, and ε investigated herein, the values of T_{Rad} obtained by solving Eq. 3 by nonlinear methods differ by less than 1 mK from those obtained with the approximation,

$$T_{\mathrm{Rad}} = \frac{T}{1 - \frac{\lambda T}{c_2} \ln(\varepsilon)} \tag{4}$$

2 Fixed-Point Blackbodies

We have five electrically heated furnaces to realize the fixed points of indium, tin, zinc, aluminum, and silver. They are all simple in their construction and conventional in their design.

The first three furnaces consist principally of an exterior cylindrical aluminum shell 330 mm in length and 203 mm in diameter containing a cylindrical aluminum block (254 mm length, 76 mm diameter) on which an electrical heater is wound. The fixed-point metal is contained within a graphite crucible held in a closed-end Pyrex tube inserted into a 52 mm diameter hole bored into the aluminum block. The space between the shell and the block is filled with Fiberfrax insulation. A 100 Ω PRT used for control purposes is inserted into a small hole drilled into the aluminum block. An inexpensive PID controller maintains the furnace within ± 0.1 °C of the set point. Girard and Ricolfi [3] have reported a furnace design of similar capability.

The higher-temperature furnaces utilize sodium-filled open-ended heat pipes to create a suitable isothermal environment for the aluminum and silver fixed points. The furnaces are water-cooled, 610 mm in length, and 305 mm in diameter. A Chromel-A heater wire is wound on an alumina former into which the sodium-filled heat-pipe furnace liner (inside diameter of 52 mm, outside diameter of 76 mm, length of 305 mm) is inserted. The graphite crucible containing the pure metal is held within a closed-end quartz tube inserted into the heat pipe such that the mid-point of the crucible is near the mid-point of the heat pipe.

All of the fixed points use graphite cavities of the same dimensions. Figure 1 illustrates the crucible design. Table 2 lists the masses of the various metals used to fill the crucibles. Figure 2 shows a zinc freeze and a melt obtained with the RT 1550; it is clearly evident that the phase transformations are resolved at the millikelvin level.

For the fixed-point blackbodies, the "reference temperature" is the freezing temperature defined by the International Temperature Scale of 1990 (ITS-90) as listed in Tables 1 and 2. Figure 6 shows the measured reflectance of our graphite sample. In the calculation of the emissivity, the cavity walls were assumed to be isothermal. For this geometry, measured reflectance, and isothermal temperature distribution, STEEP3 predicts a normal effective emissivity of 0.99934, at 1.55 µm, averaged over the central 3 mm diameter viewed by the RT1550.

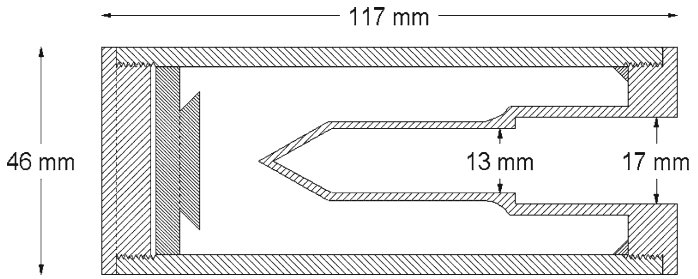

Fig. 1 Drawing of the graphite blackbody cavities used with the fixed-point furnaces

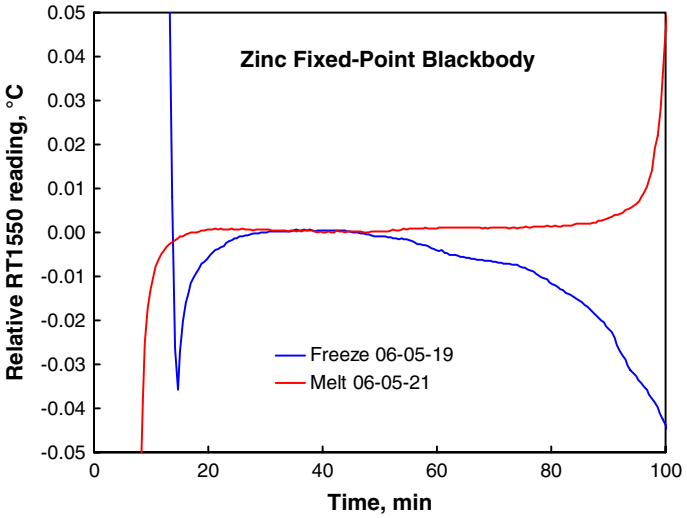

Fig. 2 Zinc freezing and melting curves as recorded by the RT1550 radiation thermometer. The high resolution and low noise of the instrument are readily apparent

Table 1 Characteristics of the blackbody sources that were involved in the intralaboratory comparison

Blackbody	Base	Aperture (mm)	Length (mm)	Temperature (°C)
Indium	Cone	13	82	156.5985
Tin	Cone	13	82	231.928
Zinc	Cone	13	82	419.527
Aluminum	Cone	13	82	660.323
Silver	Cone	13	82	961.78
Water heat pipe	Cone	52	420	50–250
Cesium heat pipe	Hemisphere	52	400	300–660
Sodium heat pipe	Re-entrant cone	55	373 (To tip of cone)	600–1000

Table 2 Fixed-point blackbody filling details

Material	Freezing temperature (°C)	Mass (g)
Indium	156.5985	689
Tin	231.928	715
Zinc	419.527	676
Aluminum	660.323	313
Silver	961.78	901

3 Variable-Temperature Blackbodies

Water-, cesium-, and sodium-filled heat pipes installed in electrically heated furnaces of our own design provide large-aperture (i.e. >50 mm) sources of blackbody radiation from 50 °C to 1000 °C. Fischer and Gutschwager [4] have described similar cesium- and sodium-filled heat pipes functioning as sources of blackbody radiation.

While the temperature of the fixed-point blackbodies can be controlled adequately with relatively simple commercial controllers, the variable-temperature blackbodies cannot benefit from the thermostatting action of a melting or freezing phase transformation. Therefore, the control system employed must be capable of providing the required temperature stability. In the case of the water-and cesium-filled heat pipes, a metal-sheathed standard platinum resistance thermometer (SPRT) connected to an ac resistance bridge is used to sense the temperature. With the sodium-filled heat pipe, a gold/platinum thermocouple connected to a nanovoltmeter is used instead. A computer reads the signal from the resistance bridge or nanovoltmeter, converts the reading to a temperature, and uses the value as input to a proportional-integral-derivative (PID) control algorithm. A digital-to-analog converter driven by the computer supplies the programming voltage for the dc power supply that energizes the heaters.

3.1 Water-Filled Heat-Pipe Blackbody

The water-filled heat pipe is constructed from Monel 400 and has an overall length of 457 mm (see Fig. 3). A SPRT serves as the sensor for the temperature controller and provides the reference temperature. The blackbody cavity is a cylinder 52 mm in diameter, terminated in a cone with an included angle of 60°, and is 420 mm in length from the apex of the cone to the aperture of the heat pipe.

The cavity was painted with Tremclad Flat Black High Heat Enamel, which the manufacturer claims resists heat to 650 °C. Figure 7 shows the reflectance measured for a sample of the paint applied to a stainless-steel disk 25 mm in diameter and 6 mm thick. The measured temperature profile along the cavity wall is shown in Fig. 9.

For this geometry, measured reflectance, and measured temperature distribution, STEEP3 predicts a normal effective emissivity of 0.99958, at 1.55 µm, averaged over the central 3 mm diameter viewed by the RT1550.

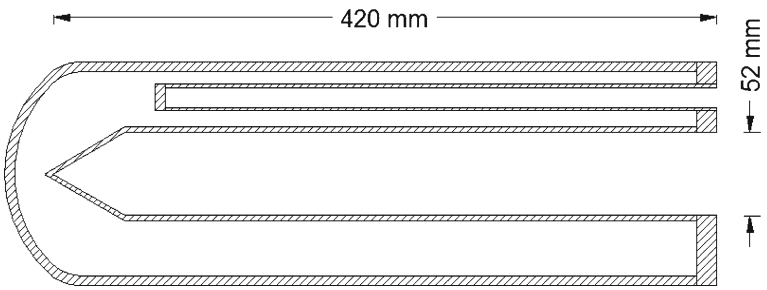

Fig. 3 Drawing of the water-filled heat-pipe blackbody source

3.2 Cesium-Filled Heat-Pipe Blackbody

The cesium-filled heat pipe is constructed from Inconel 600. The blackbody cavity is a cylinder 52 mm in diameter and terminated in a hemispherical bottom whose midpoint is 400 mm from the aperture of the heat pipe (see Fig. 4). A thermowell (not shown) houses a SPRT as the control sensor.

The cavity was painted with the same Tremclad flat black high heat enamel that was used for the water-filled heat pipe. Figure 7 indicates the measured reflectance for a sample of the paint applied to a stainless-steel disk 25 mm in diameter and 6 mm thick. The measured temperature profile along the cavity wall is shown in Fig. 9.

For this geometry, measured reflectance, and measured temperature distribution, STEEP3 predicts a normal effective emissivity of 0.99928, at 1.55 µm, averaged over the central 3 mm diameter viewed by the RT1550.

3.3 Sodium-Filled Heat-Pipe Blackbody

The sodium-filled heat pipe (see Fig. 5) was used as the blackbody source for the Fourier transform radiation thermometry project of Steele et al. [5]. The heat pipe is constructed of Inconel, a material with a relatively high emissivity when well oxidized. The cavity is 400 mm in length from the open end of the heat pipe to the base of the re-entrant cone (373 mm to the tip of the cone) and has a diameter of 55 mm.

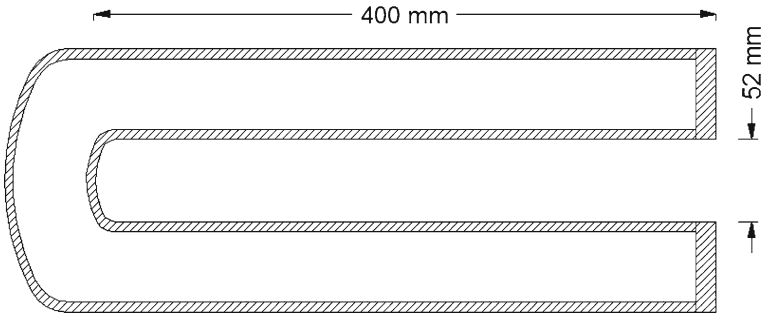

Fig. 4 Drawing of the cesium-filled heat-pipe blackbody source (thermowell not shown)

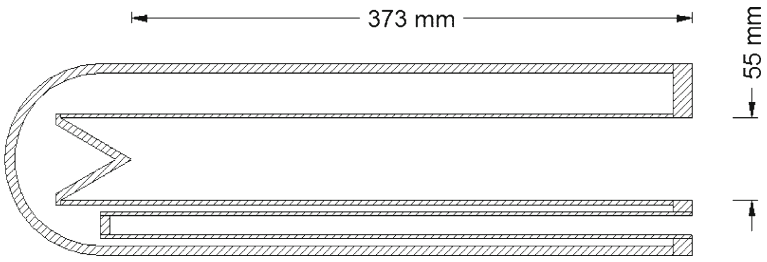

Fig. 5 Drawing of the sodium-filled heat-pipe blackbody source

The included angle of the cone is 60°. Traceability to the ITS-90 is established with a calibrated Au/Pt thermocouple that also serves as the control sensor.

Figure 8 shows the reflectance of an Inconel sample 25 mm in diameter and 3 mm thick that was cut from a baffle of a high-temperature furnace. It is assumed that the reflectance of the Inconel comprising the sodium-filled heat pipe is similar. The measured temperature profile along the cavity wall is shown in Fig. 9.

For this geometry, measured reflectance, and measured temperature distribution, STEEP3 predicts a normal effective emissivity of 0.99958, at 1.55 µm, averaged over the central 3 mm diameter viewed by the RT1550.

4 Reflectance Measurements

Reflectance measurements of the various cavity materials (graphite, Tremclad flat black high heat enamel, and Inconel) at ambient temperature were provided by the NRC Photometry and Radiometry Group.

The visible to near-infrared spectral reflectance (0.5 µm to 2.5 µm) was measured with a Perkin–Elmer Lambda-19 UV/VIS/NIR spectrophotometer equipped with a Labsphere integrating sphere accessory RSA-PE-19. The measurement geometry was 8° incidence, hemispherical collection ($8°/t$), with the specular component included.

For the infrared reflectance measurement, the sample was placed at the center of an integrating sphere with a diffuse gold-coated interior, following the configuration first proposed by Edwards [6]. The source for the modulated radiation in the reflectance apparatus was a Fourier transform infrared (FT-IR) spectrometer. The 15° incidence/total ($15°/t$) reflectance factors for the various samples are reported in Figs. 6–8.

The uncertainty of the VIS/NIR data is ± 0.005 while that of the IR data is ± 0.045.

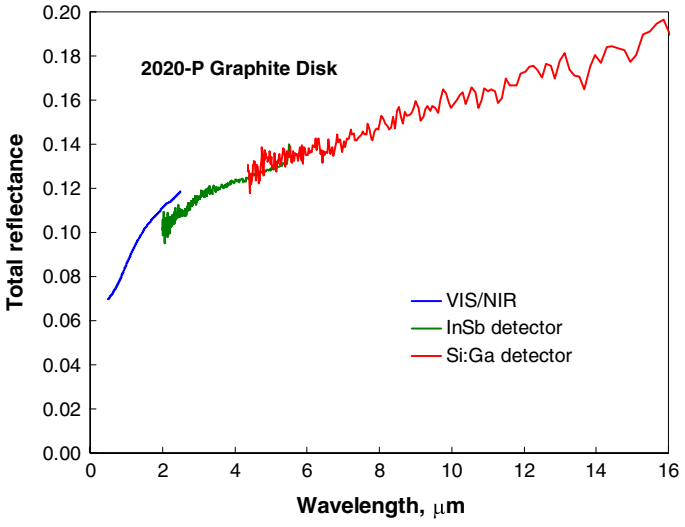

Fig. 6 Total reflectance of a graphite sample that was an actual component of the assembly of Fig. 1

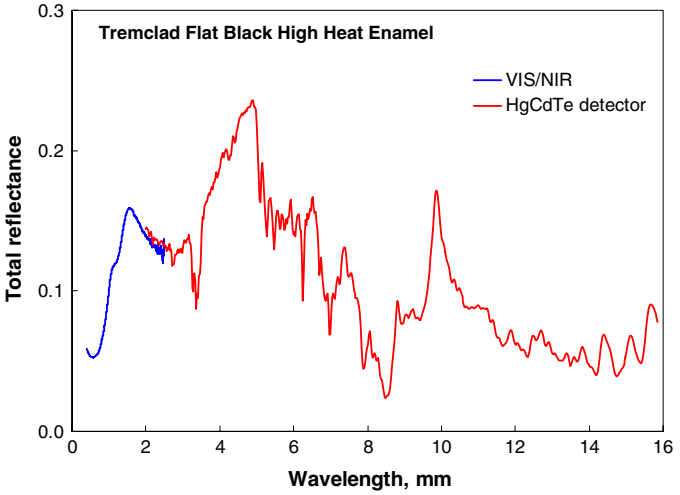

Fig. 7 Total reflectance of Tremclad flat black high heat enamel applied to a 25 mm diameter, 6 mm thick stainless-steel disk

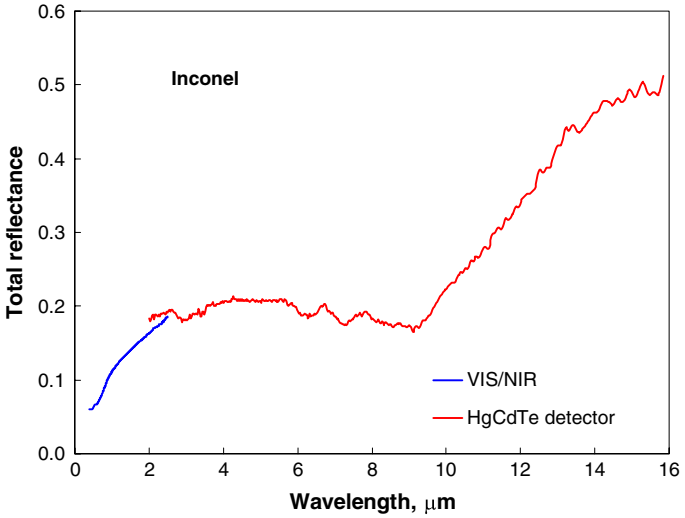

Fig. 8 Total reflectance of an Inconel sample cut from a baffle of a high-temperature furnace

5 Blackbody Wall-Temperature Distributions

The temperature gradient along the cavity wall is one of the input parameters for the calculation of the effective emissivity of the blackbody. We attempted to measure the temperature gradient along the wall by means of various thermocouple designs and also tried an optical fiber thermometer, but were finally satisfied with measuring the cavity-wall temperature using a radiation thermometer. For the water-filled heat pipe, we used the NIST RT1550. A KE LP3 Linearpyrometer operating at 899 nm and

650 nm for the cesium- and sodium-filled heat pipes, respectively was used to scan the side walls. Figure 9 shows the experimental data that were obtained.

In the case of the water-filled heat pipe, the RT1550 was tilted at angles from 0° to 10° with respect to the axis of the cavity to scan along the wall of the heat pipe. The alignment laser indicated the position of the measuring spot. For the cesium-filled heat pipe, the LP3 was tilted at an angle of approximately 6° with respect to the axis of the cavity and the LP3 was translated along the cavity axis to scan the side wall. For the sodium filled heat pipe, the LP3 was tilted at an angle of approximately 3° with respect to the axis of the cavity and the LP3 was translated along the cavity axis to scan the side wall.

6 Blackbody Comparison Measurements

The RT1550 was left on throughout the measurement period, other than when it was necessary to change rooms to access the sodium-filled heat pipe that is housed in a laboratory separate from the other blackbody sources described in this article. In this case, a stabilization time of more than 1 h was allowed before attempting any measurements.

The RT1550 was mounted on a mechanical assembly including a vertical jack and a horizontal translation stage that facilitated positioning and provided the capability to undertake vertical and horizontal scans across the apertures of the blackbody sources. A drilled mirror set at 45° to the common axis of the RT1550 and the blackbody cavity was used in conjunction with the RT1550 built-in laser to align the system as the RT1550 does not provide through-the-lens viewing. This methodology provided vertical and horizontal centering to better than 1 mm as verified by the subsequent cavity scans. The RT1550 has a fixed focal distance; therefore, to ensure that the RT1550 is focused on the plane of the source aperture, a rod of the required length is shipped with the RT1550 to verify the correct source-to-instrument spacing.

A minimum of three freeze/melt cycles were recorded for each fixed-point blackbody source. Horizontal and vertical scans with a typical resolution of 0.5 mm and 1 mm, respectively, were made during the melting plateau.

The variable-temperature blackbodies were also scanned for uniformity, extended recordings were made to assess their stability, and of course many more temperatures could be measured than were possible with the fixed-point sources. A 30-mm-diameter water-cooled aperture was placed immediately in front of the variable-temperature blackbodies and this served as the focal plane when setting the distance to the RT1550.

The measurement sequence was as follows:

1. Fixed points Sn, In, Zn, and Al
2. Sodium-filled heat pipe from 650 °C to 961.78 °C
3. Cesium-filled heat pipe from 300 °C to 660.323 °C
4. Water-filled heat pipe from 150 °C to 230 °C
5. Sodium-filled heat pipe at 650 °C and 961.78 °C (repeat measurements)
6. Ag fixed point
7. Water-filled heat pipe at 231.928 °C

7 Blackbody Uncertainty Budget

The uncertainty budget is based on the Consultative Committee for Thermometry Working Group 5 (CCT-WG5) document "Uncertainty Budgets for Calibration of Radiation Thermometers below the Silver Point" [7]. Wherever the numerical estimates of the components are given, they are to be interpreted as standard uncertainties (i.e., $k = 1$).

7.1 Calibration Temperature

This component refers to the uncertainty associated with assigning a reference temperature to the blackbody. In the case of the fixed-point blackbodies, this component is zero because the temperatures are defined by the ITS-90. For the variable-temperature blackbodies, they are the in-use uncertainties of the SPRT and the Au/Pt thermocouple. For the SPRT, the uncertainties are temperature dependent, but are estimated as less than 5 mK throughout the range of the water- and cesium-filled heat pipes. The uncertainty of the Au/Pt thermocouple used with the sodium-filled heat pipe takes into account contributions from the inhomogeneity of the thermocouple, the voltage measurement, the ice junction, etc.—we estimate a combined value of 10 mK.

7.2 Impurities

The uncertainty arising from impurities applies only to the fixed-point blackbodies and is less than 0.5 mK for tin, zinc, and aluminum. For silver, we estimate an uncertainty of 2.5 mK.

7.3 Plateau Identification

With the RT1550, the fixed-point plateaux can be identified reliably with an uncertainty of no more than 2 mK, as is apparent from Fig. 2. Nonetheless, the variability associated with repeat measurements of the freezing point must also be considered, and so we have estimated this uncertainty component as the standard deviation of the three freezes for each fixed point, and obtained values of 2 mK, 9 mK, 10 mK, 15 mK, and 41 mK for the indium, tin, zinc, aluminium, and silver fixed points, respectively.

7.4 Blackbody Emissivity, Isothermal

The fixed-point blackbodies are assumed to be isothermal as their geometry makes it difficult to scan the temperature of the cavity walls with a radiation thermometer. We use the measured reflectance of a graphite component from a crucible assembly and assume that it is representative of the behavior of the other graphite components. At 1.55 µm, the uncertainty of the reflectance is 0.0025. However, the reflectance measurements were made at room temperature so account must be made for the temperature dependence of the reflectivity. We estimate that the emissivity is accurate to

within 0.1 (full width of a rectangular distribution), and estimate the uncertainty in the emissivity accordingly. The uncertainty in the emissivity is given by

$$u\left(\varepsilon_{\mathrm{bb}}\right)=\left[\begin{array}{l}\left(\frac{1-\varepsilon_{\mathrm{bb}}}{1-\varepsilon}u\left(\varepsilon\right)\right)^{2}+\left(\left(1-\varepsilon_{\mathrm{bb}}\right)\frac{2u(L)}{L}\right)^{2}+\left(\left(1-\varepsilon_{\mathrm{bb}}\right)\frac{2u(d)}{d}\right)^{2}\\ \\ +\left(\left(1-\varepsilon_{\mathrm{bb}}\right)\cot\left(\theta\right)u\left(\theta\right)\right)^{2}+\left(\left(1-\varepsilon_{\mathrm{bb}}\right)\left(\operatorname{cosec}\left(\theta\right)-1\right)\left(\frac{\Delta t}{t}\right)^{2}\right)^{2}\end{array}\right]^{1/2} \quad (5)$$

where $\varepsilon_{\mathrm{bb}}$ is the calculated emissivity of the blackbody (0.99934), ε is the wall emissivity ($\varepsilon = 1$ – reflectance = 0.90 at 1.55 µm), $u(\varepsilon)$ is the uncertainty of the wall emissivity (0.029), L is the length of the cavity (82 mm), $u(L)$ is the uncertainty in the length of the cavity (1 mm), d is the aperture diameter (17 mm), $u(d)$ is the uncertainty of the aperture diameter (0.2 mm), θ is the cone angle (60°), $u(\theta)$ is the uncertainty of the cone angle (2.5°), Δt is the rounded area at the bottom of the cone (0.25 mm), and t is the radiation thermometer spot size at the bottom of the cavity (3 mm).

Given these input values, we obtain $u(\varepsilon_{\mathrm{bb}}) = 0.00019$. The corresponding uncertainties for the heat-pipe-based blackbodies are less.

7.5 Blackbody Emissivity, Non-isothermal

The water-, cesium-, and sodium-filled heat-pipe blackbodies are not assumed to be isothermal, but are assumed to have throughout their respective operating ranges the relative temperature distributions reported in Fig. 9. It is recognized that the effective emissivity depends on both wavelength and temperature. We have used the STEEP3 software to carry out the calculation of emissivity with the input parameters being the cavity geometry (Figs. 3–5), the measured reflectance of the wall materials (Figs. 7, 8), and the measured temperature distributions (Fig. 9). To calculate the effective emissivities, we used STEEP3 to trace 10^6 rays to calculate the average normal effective spectral emissivity for a 3 mm diameter area about the rotational axis of the cavities. The effective emissivities differ from the isothermal case by no more than 0.0004, and we are confident of the wall-temperature measurements. Therefore, a value of $u(\varepsilon_{\mathrm{bb}}) = 0.00003$ seems a reasonable estimate in accounting for the non-isothermal nature of the variable-temperature blackbodies.

7.6 Reflected Ambient Radiation

Reflected ambient radiation leads to a temperature-equivalent error given by

$$\Delta T_{\mathrm{refl}}=\frac{\lambda T_i^2}{c_2}\frac{S\left(T_a\right)}{S\left(T_i\right)}\left[1-\exp\left(\frac{-c_2}{\lambda T_i}\right)\right]\frac{\left(1-\varepsilon_{\mathrm{bb}}\right)}{\varepsilon_{\mathrm{bb}}} \quad (6)$$

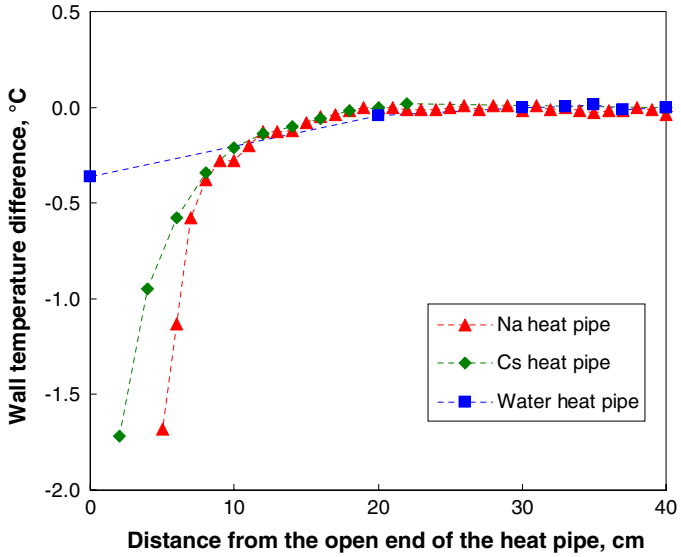

Fig. 9 The temperature distribution along the wall of the water-filled heat pipe was measured with the NIST RT1550 radiation thermometer at 1.55 µm. The temperature distribution along the wall of the cesium-filled heat pipe at 660 °C was measured using the KE LP3 radiation thermometer at 899 nm. The temperature distribution along the wall of the sodium-filled heat pipe at 962 °C was measured using the KE LP3 radiation thermometer at 650 nm

This is the required correction to the temperature measured by the radiation thermometer, and its associated uncertainty, $u(T_i)$, is given by

$$u\left(T_i\right) = \frac{\lambda T_i^2}{c_2} \frac{S\left(T_\mathrm{a}\right)}{S\left(T_i\right)} \left[1 - \exp\left(\frac{-c_2}{\lambda T_i}\right)\right] \frac{u\left(\varepsilon_\mathrm{bb}\right)}{\varepsilon_\mathrm{bb}} \tag{7}$$

T_i is the temperature of the blackbody, T_a is the ambient temperature (293 K), $S(T)$ is the signal from the blackbody at temperature T, λ is the wavelength (1.55 µm), c_2 is the second radiation constant (0.014388 m·K), and ε_bb is the calculated emissivity of the blackbody.

We assume that the ratio $S(T_\mathrm{a})/S(T_i)$ is well approximated by the following equation as the RT1550 does not produce a useful signal from sources at 293 K and we are otherwise unable to estimate $S(T_\mathrm{a})$:

$$\frac{S\left(T_\mathrm{a}\right)}{S\left(T_i\right)} = \frac{\exp\left(\frac{c_2}{\lambda T_i}\right) - 1}{\exp\left(\frac{c_2}{\lambda T_\mathrm{a}}\right) - 1} \tag{8}$$

The magnitude of the uncertainty arising from this component is negligible, being considerably less than 1 mK for the wavelength and temperatures of this comparison.

7.7 Radiant Heat Exchange

This component represents the temperature drop across the cavity bottom due to radiation exiting the cavity. An upper bound for this influence is given by the relation,

$$\Delta T_{\mathrm{b}} = \varepsilon_{\mathrm{tot}} \sigma \left(T_i^4 - T_{\mathrm{a}}^4 \right) \frac{d}{\kappa} \left(\frac{r}{L} \right)^2 \tag{9}$$

where ΔT_{b} is the temperature drop, $\varepsilon_{\mathrm{tot}}$ is the total emissivity of the cavity wall, σ is the Stefan Boltzmann constant ($5.67 \times 10^{-8}\,\mathrm{W \cdot m^{-2} \cdot K^{-4}}$), T_i is the blackbody temperature, T_{a} is the ambient temperature (293 K), d is the thickness of the cavity bottom, κ is the thermal conductivity of the cavity bottom, r is the aperture radius, and L is the cavity length (see Table 3).

The thermal conductivity of Monel is from [8]; we interpolate the values from a linear regression to the data to obtain an expression for the temperature-dependent thermal conductivity. For Inconel 600, we have likewise fit a straight line to the data of [9] and used the relation to both interpolate and extrapolate the data beyond the 20 °C to 750 °C range of the measurements.

The thermal conductivity of polycrystalline graphite is decidedly more complex than that of the aforementioned alloys, and is known to depend on how the material was made, its density, electrical conductivity, etc. (H. McEvoy and G. Machin, unpublished report). The thermal conductivity of graphite decreases in a nonlinear way above room temperature, with its value at 1000 °C being approximately half that at room temperature. This is especially unfortunate as the heat flow across the cavity bottom increases as the temperature increases, so the decreasing thermal conductivity of graphite further exacerbates the problem. Lacking direct measurements of the thermal conductivity of the graphite comprising the cavity wall, we have fit a cubic polynomial to the data of Hust and Langford [10] from 400 K to 2500 K and used the resulting equation to interpolate the values at the fixed-point temperatures.

For the purpose of calculating the temperature drop across the cavity bottom, we have estimated the total emissivity of the cavity wall as 0.85 for each of the "black" materials involved.

7.8 Convection Heat Loss

While it is recognized that convection effects may be present in the variable-temperature blackbodies of this study, no investigations of such effects have yet been carried out. We note that such effects are expected to be between 6 mK (best) and 58 mK (normal) [7] and dependent on the cavity aperture, length, and temperature. It may be worth clarifying that none of the sources described herein was operated with purging. As the cavity dimensions of the variable-temperature blackbodies of this report are all rather similar, we expect convection effects to be of similar magnitude at the temperatures of overlap. However, differences between the fixed-point and variable-temperature blackbodies may be expected due to the cavity dimensions of the fixed-point blackbodies being very much different from those of the heat-pipe-based sources. Lacking

guidance from our own measurements, we have assumed an uncertainty of 12 mK for this component for all of our variable-temperature blackbodies.

7.9 Cavity Bottom Uniformity

It is suggested [7] that this uncertainty component be calculated from the temperature variations observed by translating a radiation thermometer with a small target area across the aperture. The standard deviation of the readings across the central part corresponding to 40 % to 60 % of the area is recommended as the estimate of the uncertainty. In our case, the uncertainty evaluation was carried out by performing vertical and horizontal scans with the RT1550 across the centerline of the aperture with readings taken every millimeter. We have not, as yet, constructed a two-dimensional map of the aperture uniformity as would be suitable for a contour or three-dimensional representation of the uniformity.

For the water-filled heat pipe, the RT1550 scan showed good uniformity over a translation of 25 mm both vertically and horizontally. At 150 °C, the standard deviations were 17 mK (vertical) and 22 mK (horizontal). At 230 °C, the corresponding values were 11 mK and 6 mK.

For the cesium-filled heat pipe at 250 °C, the RT1550 scans showed good uniformity over a translation of 24 mm vertically and 19 mm horizontally, with standard deviations of 3 mK for both orientations. At 660 °C, the scans showed good uniformity over a translation of 24 mm vertically and 21 mm horizontally, with standard deviations of 12 mK and 3 mK, respectively.

For the sodium-filled heat pipe, the RT1550 scans showed good uniformity over a translation of 24 mm both vertically and horizontally, with corresponding standard deviations of 9 mK and 8 mK, respectively, at 650 °C, and 16 mK and 12 mK, respectively, at 962 °C.

7.10 Ambient Conditions

This component applies only to the variable-temperature blackbodies and is estimated from the standard deviation of the contact sensors while they are controlling at a specified set point.

For the water-filled heat pipe at 150 °C, the standard deviation indicated by the SPRT was 10 mK for a monitoring period of 106 minutes and that of the RT1550 readings was 28 mK. At 230 °C, the corresponding values were 8 mK (SPRT) and 4 mK (RT1550) for a monitoring period of 70 min.

For the cesium-filled heat pipe at 250 °C, the standard deviation of both the SPRT and RT1550 readings for a period of 13 min was less than 1 mK. The standard deviations of the RT1550 remain of the order of a few mK up to 660 °C, and were no more than 3 mK for all of our measurements with the cesium-filled heat pipe.

For the sodium-filled heat pipe at 650 °C, the standard deviation indicated by the Au/Pt thermocouple for a monitoring period of 100 min was 6 mK and that of the RT1550 readings was 7 mK. At 962 °C, the corresponding values were 4 mK (Au/Pt thermocouple) and 7 mK (RT1550) for a monitoring period of 23 min.

8 Uncertainties of the Radiation Thermometer

In [7], the uncertainties attributable to the radiation thermometer are the size-of-source effect, nonlinearity, the effect of the instrument temperature, atmospheric absorption, gain ratios, and noise. Interpolation error and drift also require consideration.

The size-of-source effect (SSE) is of no consequence when comparing the various variable-temperature blackbodies as the same limiting aperture was placed in front of all of them. However, the fixed-point blackbodies are of smaller diameter, so a difference could arise with respect to the variable-temperature blackbodies due to the SSE. Fortunately, the RT1550 has a small target area. Our measurements indicate that its temperature indication is invariant for source diameters from 7 mm to 30 mm. Therefore, we consider the uncertainty arising from the SSE to be negligible.

Non-linearity is not a factor in the comparison of blackbody sources at the same temperature, though it may contribute to the 'shape' of the temperature differences at temperatures between the fixed points. For the purposes of the comparison, we consider the uncertainty attributable to this component to be negligible.

The laboratory temperature ranged from 20 °C to 24.2 °C throughout the course of the measurements. By plotting the RT1550 reading versus laboratory temperature for the fixed-point data and the four measurements of the cesium-filled heat pipe at 660.323 °C, it is evident (in *nearly* all cases) that the RT1550 exhibits a negative temperature coefficient. Unfortunately, the scatter in the apparent temperature coefficients makes estimation of the temperature sensitivity of the RT1550 rather challenging, although the change in the output may be of order 0.025 °C per degree Celsius change in room temperature.

Atmospheric absorption effects can be expected to be negligible at 1.55 µm as it is within a window of high atmospheric transmission. In addition, the short path length minimizes the sensitivity to such effects. The relative humidity varied between 32 % and 60 % during the course of the measurements; however, we have no evidence to suggest that these variations contributed to the uncertainty of the observed differences.

Six gain changes in the RT1550 amplifier were required to cover the temperature range from 150 °C to 962 °C. We are of the opinion that the uncertainty arising from changes of gain has negligible influence on the uncertainty of the blackbody comparison.

The noise of the radiation thermometer contributes to the uncertainty of the comparison, but we must be careful not to count this component twice. In Sect. 7.10, we attribute what may be better described as noise arising from the RT1550 to the influence of ambient conditions on the blackbody. Because this uncertainty component has already been assigned to the blackbody, we do not feel that it should be included again.

The RT1550 is used primarily as a comparator in this exercise. Interpolation error is not a factor in the comparison of blackbody sources at the same temperature, although it may contribute to the 'shape' of the temperature differences at temperatures between the fixed points upon which its calibration was based. Lacking information to the contrary, we consider the uncertainty attributable to this component to be negligible.

Drift in the RT1550 over the two months of the comparison may contribute to the scatter in the measurements, but we are unable to resolve such a drift, e.g., within the scatter of the repeat measurements of the sodium-filled heat pipe.

Table 3 Characteristics of the blackbody sources that were involved in the intralaboratory comparison

Parameter	Fixed-point	Water	Cesium	Sodium
Wall material	Graphite	Monel 400 + paint	Inconel + paint	Inconel
$\varepsilon_{\mathrm{tot}}$	0.85	0.85	0.85	0.85
d (mm)	2	3	3	3
$\kappa(\mathrm{W}\cdot\mathrm{m}^{-1}\cdot\mathrm{K}^{-1})$	89–49	23–29	17–25	25–31
r (mm)	8.5	26	26	27.5
L (mm)	82	420	400	373
T_i (K)	430–1235	323–523	543–933	923–1273
ΔT_{b} (mK)	0–46	0–1	3–17	22–62

Table 4 Uncertainty budget for the NRC fixed-point blackbody sources at 1.55 μm

Source	Indium	Tin	Zinc	Aluminum	Silver
t (°C)	156.5985	231.928	419.527	660.323	961.78
Reference temperature (mK)	0	0	0	0	0
Impurities (mK)	0.5	0.5	0.5	0.5	2.5
Plateau identification (mK)	2	9	10	15	41
Blackbody emissivity, isothermal (mK)	4	5	10	18	32
Reflected ambient radiation (mK)	0	0	0	0	0
Cavity bottom heat exchange (mK)	0	0	2	8	28
Combined uncertainty ($k = 1$) (mK)	4	10	14	25	59
Expanded uncertainty ($k = 2$) (mK)	9	21	29	50	118

As the RT1550 is used primarily as a radiance comparator, noise and drift might be expected to be combined to form the uncertainty of the comparison, but we have already included the noise component in the blackbody uncertainty budget and we have no evidence of drift. In summary, we are of the opinion that the uncertainties listed in Tables 4 and 5 include the uncertainties of the comparison process, with the possible exception of the temperature coefficient of the RT1550.

9 Results

The data summary of Fig. 10 compares the readings of the RT1550 with various reference temperatures (the assigned ITS-90 temperatures in the case of the fixed points, the temperatures from an SPRT calibrated in accordance with the ITS-90 for the water- and cesium-filled heat-pipe blackbodies, and the temperatures from a calibrated Au/Pt thermocouple for the sodium-filled heat-pipe blackbody) corrected for the effective emissivity of the respective blackbody. The "baseline" for the graph is, effectively, the NIST calibration of the RT1550. The error bars indicated in the figure are the uncertainties of the blackbodies from Tables 4 and 5.

Table 5 Uncertainty budget for the NRC variable-temperature blackbody sources at 1.55 µm

Source	Water		Cesium		Sodium	
t (°C)	150	230	300	660	650	962
Reference temperature (mK)	5	5	5	5	10	10
Blackbody emissivity, isothermal (mK)	2	2	5	12	8	14
Blackbody emissivity, non-isothermal (mK)	1	1	1	3	3	5
Reflected ambient radiation (mK)	0	0	0	0	0	0
Cavity bottom heat exchange (mK)	0	1	2	11	13	38
Convection (mK)	12	12	12	12	12	12
Cavity bottom uniformity (mK)	28	8	3	12	9	16
Ambient conditions–stability (mK)	10	8	1	3	7	7
Combined uncertainty ($k = 1$) (mK)	33	17	14	25	25	47
Expanded uncertainty ($k = 2$) (mK)	65	35	29	49	49	94

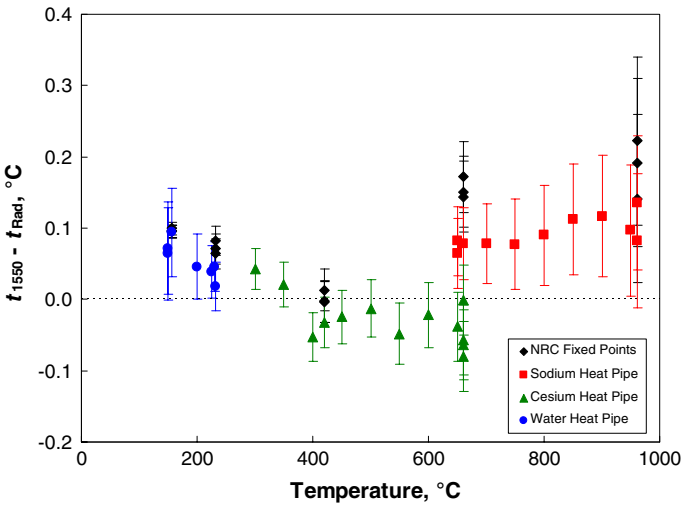

Fig. 10 Temperature differences at the various thermometer calibration points, where t_{1550} is the value indicated by the RT1550 and t_{Rad} is the radiance temperature of the blackbody (reference temperature corrected for the effective emissivity)

The fixed-point and variable-temperature blackbody sources differ by not more than ± 0.13°C from 150 °C to 962 °C, and in most cases, the agreement is considerably better. The largest discrepancy is near 660 °C and manifests itself as a difference of approximately 0.12 °C between the cesium- and sodium-filled heat pipes, and the aluminum fixed point is approximately 0.2 °C different from the cesium-filled heat pipe. A definitive explanation for the difference remains to be determined. Empirically, we find that the cesium- and sodium-filled heat-pipe data can be reconciled if the effective emissivity of the cesium-filled heat pipe is changed from 0.99928 to 0.998, though we have no basis for doing so. Likewise, increasing the effective emis-

sivity of the fixed-point blackbodies from 0.99934 to 0.9997 generally improves their agreement with the variable-temperature blackbodies.

To further probe the apparent temperature differences, we compared the cesium- and sodium-filled heat pipes, with their set points at 660.323 °C, with the aluminum fixed-point blackbody using our KE LP3 Linearpyrometer operating at 899 nm. At this wavelength, the emissivities are 0.99966 (Cs heat pipe), 0.99971 (Na heat pipe), and 0.99949 (Al fixed point), so the corresponding radiance temperatures are 660.304 °C, 660.307 °C, and 660.295 °C. The apparent temperatures of the various sources were determined, and the differences calculated with respect to the respective radiance temperatures. With the aluminum fixed-point measurements as the baseline, we find the cesium-filled heat pipe to be 75 mK colder and the sodium-filled heat pipe 85 mK hotter (Cs and Na differ by 160 mK). A similar analysis using the RT1550 with the aluminum fixed-point values as the baseline shows the cesium-filled heat pipe to be 206 mK colder and the sodium-filled heat pipe 77 mK colder (Cs and Na differ by 129 mK). The LP3 values do not appear to confirm the differences determined with the RT1550, though the difference between the cesium-and sodium-filled heat pipes (160 mK versus 129 mK) is probably within the reproducibility of the measurements for $k = 2$.

10 Conclusion

From the experimental data reported here, the temperature differences among our various sources are most apparent near 660 °C, and this suggests that further investigations of the effective emissivities of our blackbody sources are required. We are currently evaluating the feasibility of setting up a system at NRC for the direct determination of blackbody cavity emissivity, following the NIST methodology [11]. Because at least a portion of the apparent temperature differences may be due to the influence of changes in room temperature on the output of the RT1550, we will repeat the comparison measurements once we receive delivery of the RT1550 that we have purchased from NIST.

At this point, we believe that sufficient evidence is in hand to conservatively claim that the blackbody sources investigated herein are compatible within the bounds ±0.2 °C. As a goal to guide future work, we seek to advance our understanding of their behavior such that the apparent differences in radiance temperature become less than ±0.05 °C.

Acknowledgments The authors would like to express their thanks to Mario Noel (VIS/NIR) and Nelson Rowell (IR) of the NRC Photometry and Radiometry Group for the reflectance measurements reported in this article. We are grateful to Sergey Mekhontsev and Leonard Hanssen of NIST for the loan of the RT1550 radiation thermometer for a period of several months during which the measurements of the blackbodies were made.

References

1. K.D. Hill, D. J. Woods, in *Temperature, Its Measurement and Control in Science and Industry*, vol. 7, ed. by D.C. Ripple (AIP, Melville, New York, 2003), pp. 669–674

2. M. Noorma, S. Mekhontsev, V. Khromchenko, A. Gura, M. Litorja, B. Tsai, L. Hanssen, in *Proceedings of Thermosense XXVIII*, ed. by J.J. Miles, G.R. Peacock, K.M. Knettel, Proc. SPIE, vol. 6205 (SPIE, 2006). doi:10.1117/12.667253
3. F. Girard, T. Ricolfi, Meas. Sci. Technol. **9**, 1215 (1998)
4. J. Fischer, B. Gutschwager, in *Proceedings of TEMPMEKO '96, 6th International Symposium on Temperature and Thermal Measurements in Industry and Science*, ed. by P. Marcarino (Levrotto and Bella, Torino, 1997), pp. 251–256
5. A.G. Steele, P.C. Dufour, N.L. Rowell, in *Proceedings of TEMPMEKO '99, 7th International Symposium on Temperature and Thermal Measurements in Industry and Science*, ed. by J. F. Dubbeldam, M.J. de Groot (Edauw Johannissen bv, Delft, 1999), pp. 720–725
6. D.K. Edwards, J.T. Gier, K.E. Nelson, R.D. Roddick, J. Opt. Soc. Amer. **51**, 1279 (1961)
7. J. Fischer, P. Saunders, M. Sadli, M. Battuello, C.W. Park, Yuan Zundong, H. Yoon, Wang Li, E. van der Ham, F. Sakuma, Y. Yamada, M. Ballico, G. Machin, N. Fox, J. Hollandt, M. Matveyev, P. Bloembergen, S. Ugur, *Uncertainty Budgets for Calibration of Radiation Thermometers below the Silver Point*, CCT-WG5 on Radiation Thermometry, Version 1.71, Final Version, April 2008 (http://www.bipm.org/wg/CCT/CCT-WG5/Allowed/Miscellaneous/Low_T_Uncertainty_Paper_Version_1.71.pdf)
8. http://www.hightempmetals.com/techdata/hitempMonel400data.php
9. J. Clark, R. Tye, High Temp.-High Press. **35/36**, 1 (2003/2007)
10. J.G. Hust, A.B. Lankford, *National Bureau of Standards Report of Investigation, Research Materials 8424, 8425, and 8426, Graphite Thermal Conductivity and Electrical Resistivity as a Function of Temperature from 5 to 2500 K* (1984). https://srmors.nist.gov/reports/8424.pdf?CFID=16546233&CFTO-KEN=ee725e58201bc5f2-532055AE-9ABD-0A16-67C8A200CEA-EE842&jsessionid=b4307e26d9a61a3a7248
11. L.M. Hanssen, S.N. Mekhontsev, J. Zeng, A.V. Prokhorov, in *Proceedings of TEMPMEKO 2007*, Int. J. Thermophys. **29**, 352 (2008). doi:10.1007/s10765-007-0314-8